

# Flood Disaster Rapid Simulation and Risk Assessment Technology Based on Spatiotemporal Data

Kui Zhang, Yingchun Tao,\* Xuping Zhang, Yanyan Zeng,\*\*  
Zongxia Xu, Hanmei Liang, and Yandi Zhou

Beijing Institute of Surveying and Mapping, No. 15, Yangfangdian Road, Haidian District, Beijing 100038, China

(Received August 9, 2024; accepted March 18, 2025)

**Keywords:** flood disasters, spatiotemporal data, rapid simulation of inundation, damage assessment, hazard assessment

With global warming, flood disasters caused by rainstorms have been occurring frequently in recent years. Therefore, it is necessary to carry out disaster loss and risk assessment. How to quickly and accurately achieve disaster risk assessment is a major problem in risk assessment work. In this paper, we constructed a disaster risk assessment and disaster area risk prediction analysis model from the two aspects of loss degree and danger in disaster risk assessment. First, we realized the rapid simulation of inundation area, inundation depth, and flow velocity by using the inundation simulation and estimation model of flood disaster. Second, on the basis of simulation results of the flooding model, combined with multisource spatiotemporal data, we constructed a dynamic assessment model for disaster losses and a bridge hazard analysis model to effectively evaluate the spatial distribution of damaged buildings, construction land, agricultural land, and bridges in a disaster area. Third, in this paper, we propose a disaster risk prediction and analysis technique to predict the spatial distribution of areas potentially affected by rainfall. Finally, we selected three regions in Beijing as experimental areas, namely, Mentougou District, Fangshan District, and Changping District, where an extremely heavy rainstorm occurred in July 2023. On the basis of the above models, the risk assessment and prediction analysis of rainstorm disasters were carried out, which proved that the models proposed can provide data support for rapid disaster assessment and leadership decision-making to a certain extent.

## 1. Introduction

Rainfall is a common natural disaster, which has a wide range of impacts and destructive power, and poses a serious threat to urban transportation, public facilities, and residents' lives.<sup>(1)</sup> Rapid and accurate rainstorm disaster risk analysis can provide not only timely and effective data support for rescue workers, but also technical support for the precise delivery of relief materials, and it can also improve the efficiency of postdisaster rescue.<sup>(2)</sup> Therefore, how to achieve rapid and accurate disaster risk analysis is one of the current research problems. An

---

\*Corresponding author: e-mail: [527359590@qq.com](mailto:527359590@qq.com)

\*\*Corresponding author: e-mail: [zengyanyan1989@163.com](mailto:zengyanyan1989@163.com)

<https://doi.org/10.18494/SAM5295>

accurate disaster risk assessment model can provide data support for postdisaster reconstruction and leadership decision-making.

Loss degree is the main outcome of disaster risk analysis, which mainly refers to the spatial location and intensity of rainstorm inundation in the analysis and evaluation of the impact of heavy rainfall.<sup>(3)</sup> Combined with the data of buildings, roads, bridges, and other affected infrastructure, a correlation analysis model of multisource spatiotemporal data and rainstorm-inundated location and intensity was constructed in order to quickly and accurately assess the loss and risk analysis of various facilities caused by a rainstorm.<sup>(4–7)</sup> Therefore, accurate disaster simulation estimation is the basis for constructing the correlation analysis model, which affects the speed and accuracy of constructing the correlation model between the simulation estimation results and the spatiotemporal data.

The simulation and estimation of heavy rainstorm disaster are mainly performed by combining extreme hydrometeorological data with hydrological models, including probability statistics and model simulation. The probability statistics method is based on historical disaster data to calculate the loss caused by disasters. Owing to the lack of data, this method can only be evaluated on a large scale.<sup>(8,9)</sup> The model simulation method is used to study the disaster loss from the objective empirical analysis and simulation of the physical mechanism of the disaster, which has higher accuracy and authenticity than the probability statistics method. It mostly adopts spatial analysis and hydrological models for simulation, such as determining the relationship between the highest water level and the high-precision digital elevation model (DEM), and quickly obtains the inundation depth.<sup>(10–12)</sup> Some scholars coupled the stormwater control measure model with the flood area model to conduct the rapid simulation and estimation of disaster.<sup>(13)</sup> Yang *et al.* used the coupled 1D and 2D SOBEK hydrodynamic models to simulate flood inundation.<sup>(14)</sup> Wu *et al.* used the dominant river tracing-routing integrated with variable infiltration capacity (VIC) environment (DRIVE) model and its global-to-local real-time flood forecasting system to simulate the spatial distribution of inundation of heavy rainfall by inputting meteorological elements, including precipitation, wind speed, and temperature, and land surface parameter sets such as soil, vegetation, and topography. The model realizes the rapid simulation of the dynamic process and spatial and temporal distributions of disasters.<sup>(15–19)</sup>

Therefore, to quickly and accurately realize the disaster loss assessment caused by heavy rainfall, we first adopted the DRIVE hydrological model to simulate the inundation area, inundation depth, and maximum flow rate of floods, so as to quickly obtain the spatial distribution of the inundation caused by heavy rainfall. Second, on the basis of the spatial distribution range of inundation, combined with spatial and temporal data such as topography, construction, and land use in Beijing, we constructed the dynamic analysis model of disaster loss and the bridge risk analysis model to realize the immediate assessment of disaster damage. Finally, on the basis of the above models, we put forward a disaster early warning and assessment model and took Fangshan District as a test area to forecast and analyze the rainfall disaster.

## 2. Methods

First, we obtained the location and affected area of the disaster, established relatively reliable original basic data, and combined the DEM topographic data, as well as the meteorological data

such as rainfall, air temperature, and wind speed, and through the inundation simulation estimation model, we realized the data of the inundation range, inundation depth, and flood flow velocity in the affected area. Second, on the basis of the inundation range and depth data simulated by the model, combined with multisource spatial and temporal data such as houses, construction land, agricultural land, and unused land, and using the multiscale grid as the dividing unit, we constructed the dynamic assessment model of disaster damage, which is used to assess and analyze the loss degree of a disaster area. Third, on the basis of the flood velocity data simulated by the inundation simulation estimation model, we constructed the bridge risk analysis model to analyze and evaluate the bridge affected by the flood. Fourth, on the basis of the above model identification results, combined with the hourly inundation range simulated by the model, we predicted the degree of damage to the suspected disaster area caused by precipitation, which proved the practicability of each analysis and assessment model constructed in this paper, and at the same time, proved that our analytical model has the ability of rapid response to disaster risk assessment. The research idea of this paper is shown in Fig. 1.

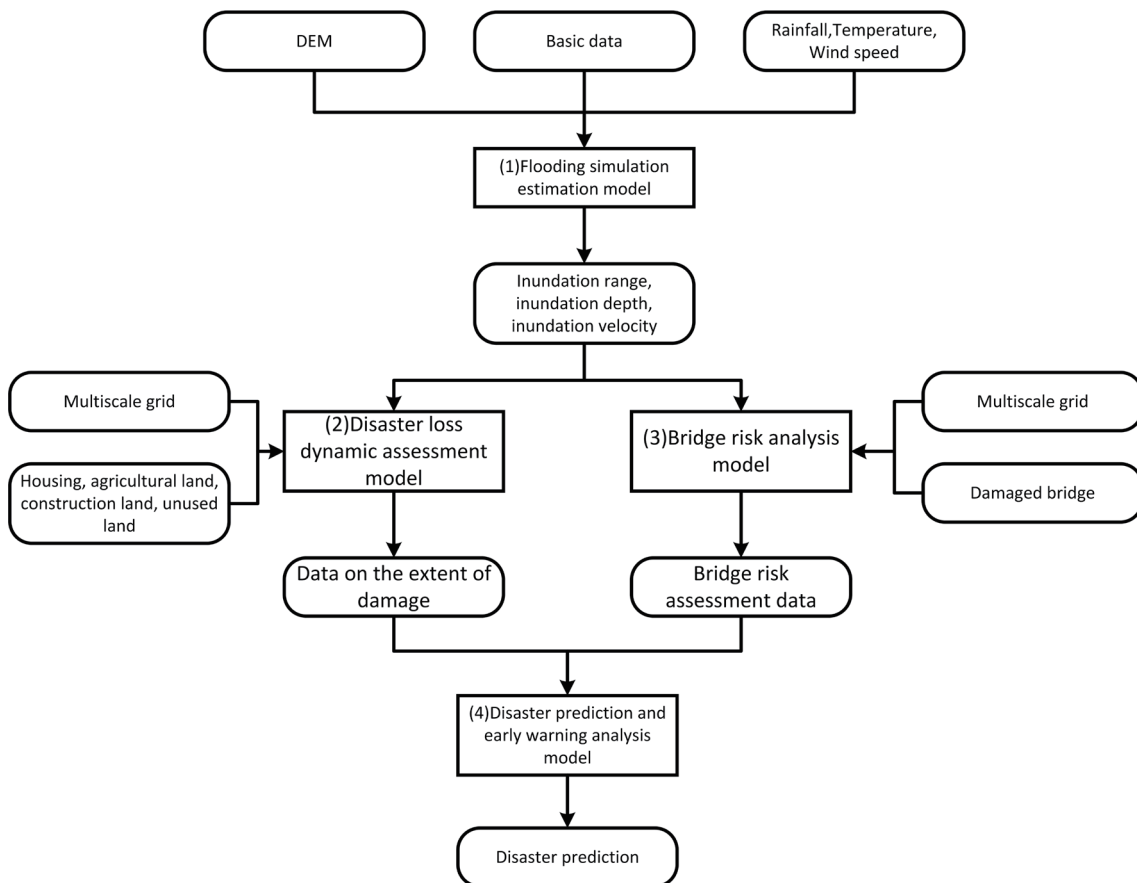


Fig. 1. Technical road map for model construction.

## 2.1 Estimation model for flood simulation

The DRIVE model used in this paper is a coupling of the large-scale distributed hydrologic VIC and DRTR models. The DRTR model calculation formula is

$$\text{Continuity equations: } \frac{\partial A}{\partial t} + \frac{\partial Q}{\partial x} = q_L, \quad (1)$$

$$\text{Momentum equation: } S_f = S_0, \quad (2)$$

$$\text{Manning's formula: } Q = \frac{S_0^{1/2}}{nP^{2/3}} A^{5/3}, \quad (3)$$

where  $t$  is time (s),  $x$  is the longitudinal flow distance (m),  $A$  is the wetted area ( $\text{m}^2$ ) defined as the cross-sectional area of the channel below the surface of the water,  $P$  is the wetted perimeter (m), and  $S_f$  is the friction slope that combines the effects of gravity, friction, inertia, and other forces on the water surface. If the terrain is steep enough for gravity to play a greater role than other forces, then  $S_f$  can be approximated using the channel bottom slope  $S_0$ , which is a basic assumption of the kinematic wave routing method. In Eq. (3),  $n$  is Manning's roughness coefficient, which is not directly measurable and is mainly controlled by surface roughness, bottom material type, flow channel curvature, and so forth.  $Q$  is the flow rate ( $\text{m}^3/\text{s}$ ) and  $q_L$  is the lateral flow rate per unit width ( $\text{m}^3/\text{s}/\text{m}$ ).

## 2.2 Dynamic assessment model of disaster losses

On the basis of the data of inundation range and depth simulated in Sect. 1.2, combined with the number of houses, agricultural land, construction land, and unused land, we constructed the dynamic assessment model of disaster damage to realize the rapid assessment of the disaster situation in the disaster area under heavy rainfall disaster. First, we constructed a multiscale analysis grid spatial unit, which is the analysis unit of the model in this paper. Second, we processed and analyzed the submergence data and the spatiotemporal data of disaster facilities on the basis of the spatial unit and obtained the submergence simulation data of a multiscale grid. Finally, on the basis of the multiscale grid data, we used the spatial overlay analysis and grid statistics technology to quickly assess the damaged area of the building, the number of houses, agricultural land, construction land, and unused land, and the disaster situation is analyzed immediately after the disaster occurred. The affected areas of construction land, agricultural land, and unused land are the data areas in the statistical grid, and the number of houses is the number of affected areas in the statistical grid. The affected building area is the building area within the statistical grid, and the formula for the affected building area within each grid is

$$\text{Building Area}_i = \sum_{k=0}^n A_k * C_k, \quad (4)$$

where  $Building\ Area_i$  represents the area of the damaged building in the  $i$  grid,  $n$  represents the number of damaged buildings,  $A_k$  represents the bottom area of the  $K$  building, and  $C_k$  represents the number of floors of the  $K$  building.

### 2.3 Bridge hazard analysis models

On the basis of the flow velocity data of the simulated inundation area in Sect. 1.2, we interpreted the data of the bridge that is clearly affected by the disaster through remote sensing. Then, we determined and analyzed the correlation between the flow velocity and the data of the damaged bridge. This correlation model can evaluate the disaster-hit bridges that cannot be identified by remote sensing, analyze the bridges that are subject to greater impact by the flood water during the occurrence of the rainstorm, and conduct the hazard analysis and evaluation of the bridges within the disaster area. We carried out the risk analysis and evaluation of bridges in the disaster-affected area to provide data support for the rapid analysis of the damage of bridges after the disaster. Through the intersection of bridge and flow velocity data, the number of grids ( $N$ ) where the bridge is located and the corresponding flow velocity  $V$  of each grid are obtained, and the average flow velocity of the bridge is calculated.

$$AV_i = \sum_{j=0}^n V_{ij} / N_i \quad (5)$$

Here,  $AV_i$  represents the average flow velocity of bridge  $i$  and  $V_{ij}$  represents the flow velocity of the  $j$  grid within bridge  $i$ .  $N_i$  is the number of grids covered by bridge  $i$ .

## 3. Experiments and Analysis

### 3.1 Dataset

On July 29, 2023, under the effect of the residual circulation of Super Typhoon Doksuri and the subtropical high pressure, the water vapor transport of Super Typhoon Khanun, and the comprehensive effect of topography, severe heavy rain occurred in Beijing and its surrounding areas, accompanied by major floods, among which Mentougou District, Fangshan District, and Changping District were affected very seriously than other districts. These districts are located in the west of Beijing. The topography is relatively undulating and the mountainous area is relatively large, among which the mountainous area of Fangshan District is about 1327 square kilometers. The Mentougou mountainous area accounts for 98.5%, and the mountainous area of Changping District is about 800 square kilometers.

Therefore, we took the three severely affected areas of Mentougou District, Fangshan District, and Changping District in Beijing as the study areas. The data used in this study included inundation-related and multisource spatiotemporal data. Among them, the resolution of terrain data is 2 m, the grid resolution of rainfall inundation data simulated by the inundation simulation model is 90 m, and the time resolution of rainfall inundation data is from 8:00 p.m. on July 23 to 8:00 p.m. on August 6, 2023. Combined with meteorological data such as precipitation

and temperature and topographic data, the inundation simulation estimation model constructed and described in Sect. 2.2 is used to simulate the maximum inundation area where flooding occurs, and then combined with the spatial and temporal data of housing and land use in Beijing, the dynamic assessment model of disaster damage constructed and described in Sect. 2.3 is used to evaluate the affected building area and farmland. Combined with the partially damaged data of bridges decoded from satellite remote sensing, the risk evaluation model of bridges constructed and described in Sect. 2.4 is applied to evaluate the riskiness of bridges. Combined with some bridge damage data decoded by satellite remote sensing, the correlation between bridge damage and water flow rate is analyzed using the bridge risk evaluation model constructed and described in Sect. 2.4.

## 3.2 Experimental results

### 3.2.1 Flood simulation estimation model analysis results

The inundation simulation and estimation model described in Sect. 2.1.2 was used to simulate the inundation range and impact in Mentougou District, Fangshan District, and Changping District (Fig. 2). The analysis result shows that the spatial distribution of inundation water depth exceeded 500 mm in Mentougou District, Fangshan District, and Changping District (i.e., the disaster-affected areas adopted in this analysis) (Fig. 3). Figure 3 shows that the maximum

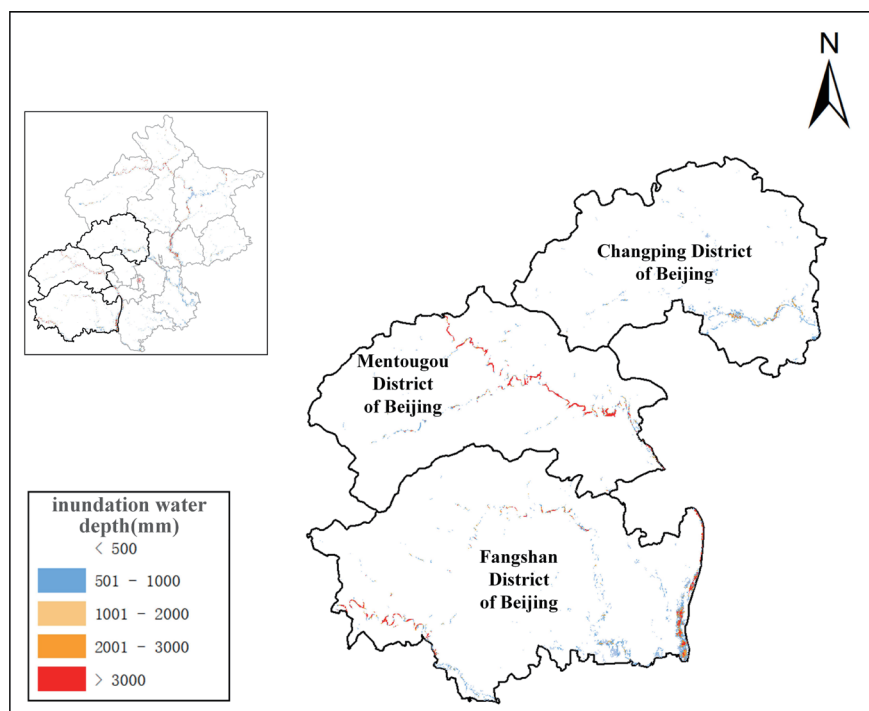


Fig. 2. (Color online) Distribution of inundation water depth from 8 pm July 23, 2023 to 8 pm August 6, 2023 in Fangshan District, Mentougou District, and Changping District (mm).

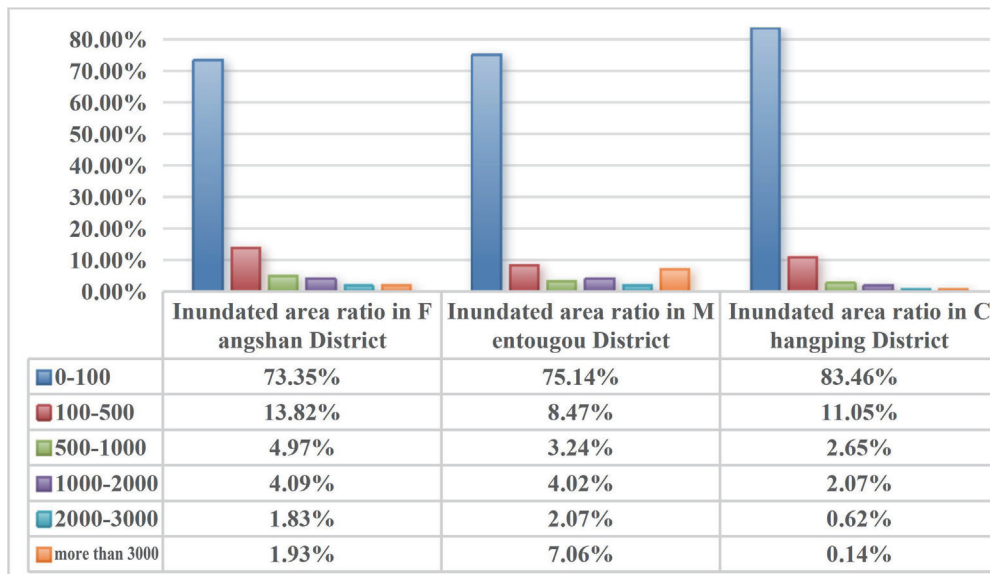


Fig. 3. (Color online) Statistics of inundated area ratio in Fangshan District, Mentougou District, and Changping District.

inundation water depth is located in Mentougou District, and Fangshan District not only has a larger inundation water depth but also a larger disaster-affected area. After comparison with the results of radar image analysis and preliminary manual judgment, the main trends of the estimation results were found to be basically consistent with the actual situation.

### 3.2.2 Results of the dynamic assessment model for disaster losses

#### 3.2.2.1 Results of the dynamic assessment of disaster losses in Fangshan District

Through the loss analysis of building area, quantity, and land type in Fangshan District, we saw that Fangshan District is the most seriously affected among the three districts, and the affected areas of construction land, agricultural land, and buildings are larger than those of the other two districts. In addition, the inundation area of Fangshan District is not only wide but also deep (Fig. 4). The affected area of construction land with a larger submerged water depth accounts for about 4% of the total affected area of construction land, and agricultural land accounts for about 2.3% of the total affected area of agricultural land. The number of affected houses is large, accounting for about 3% of the total number of affected houses (Fig. 5).

#### 3.2.2.2 Mentougou District results of the dynamic assessment of disaster losses

On the basis of the dynamic assessment model of disaster damage in Sect. 2.1.3, we analyzed the disaster situation of construction area, quantity, and land use in Mentougou District. We saw that Mentougou District is the more seriously affected among the three districts. The spatial

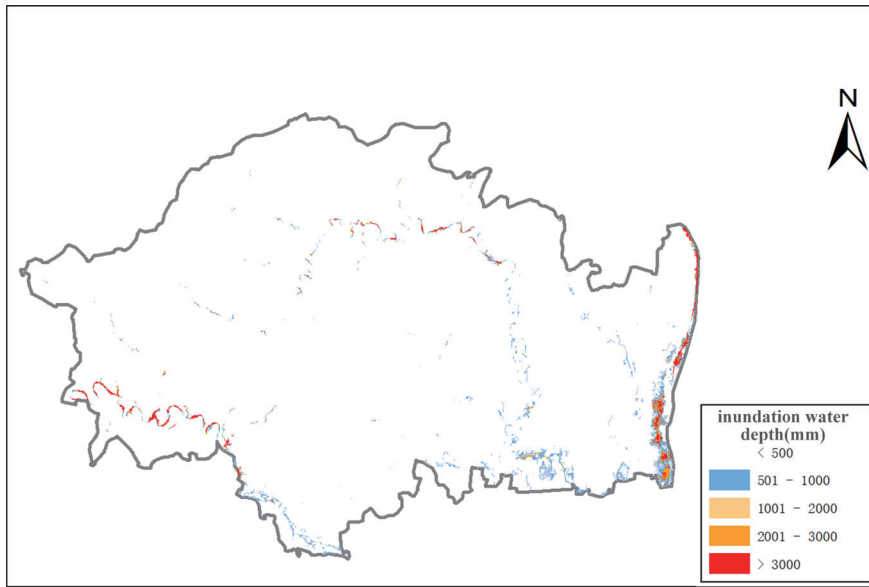


Fig. 4. (Color online) Distribution of inundation water depth from 8 pm July 23, 2023 to 8 pm August 6, 2023 in Fangshan District (mm).

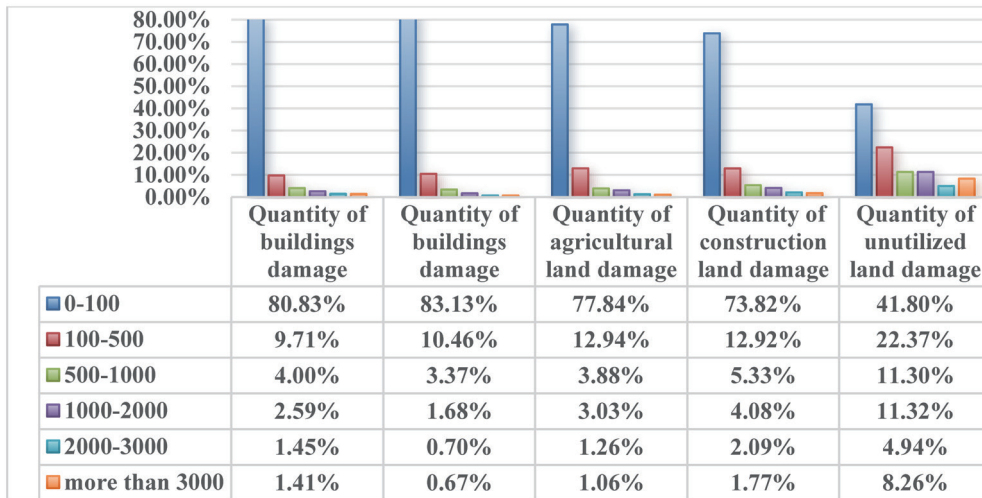


Fig. 5. (Color online) Statistical map of damage in Fangshan District.

distribution of inundation depth is shown in Fig. 6. Figure 7 shows the damage of construction land, agricultural land, the number of buildings, and construction area. The total area of severely affected construction land and agricultural land in Mentougou District is less than that in Fangshan District, accounting for 55% of the total area of construction land and agricultural land, respectively, and the number of affected buildings accounts for 46% of the total number of affected houses.

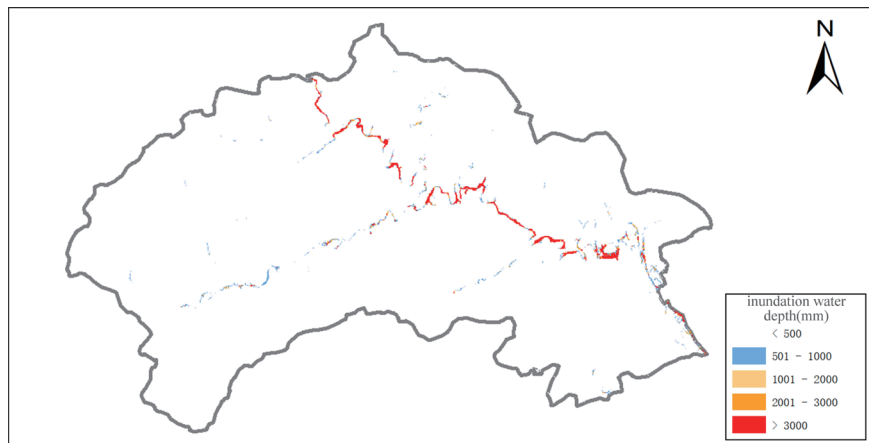


Fig. 6. (Color online) Distribution of inundation water depth from 8 pm July 23, 2023 to 8 pm August 6, 2023 in Mentougou District (mm).

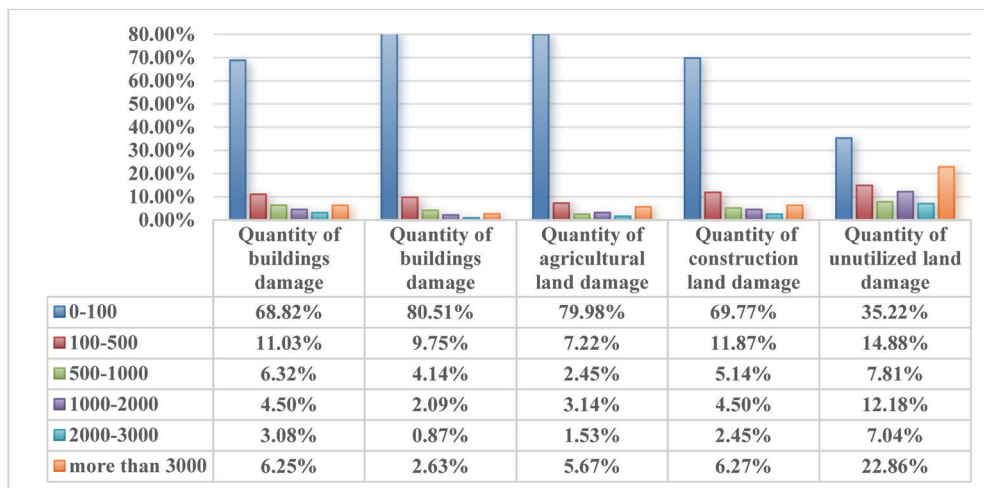


Fig. 7. (Color online) Statistical map of damage in Mentougou District.

### 3.2.2.3 Results of the dynamic assessment of damage in Changping District

According to the dynamic assessment model of disaster loss in Sect. 2.1.3, Changping District is the least affected among the three districts (Fig. 8). The quantities of construction land, agricultural land, and buildings affected by the disaster are shown in Fig. 9. The inundated water depth in most areas of Changping District is small, and the inundated water depth of more than 2000 mm accounts for 5% of the total construction land area, 15% of the agricultural land area, and about 4% of the buildings.

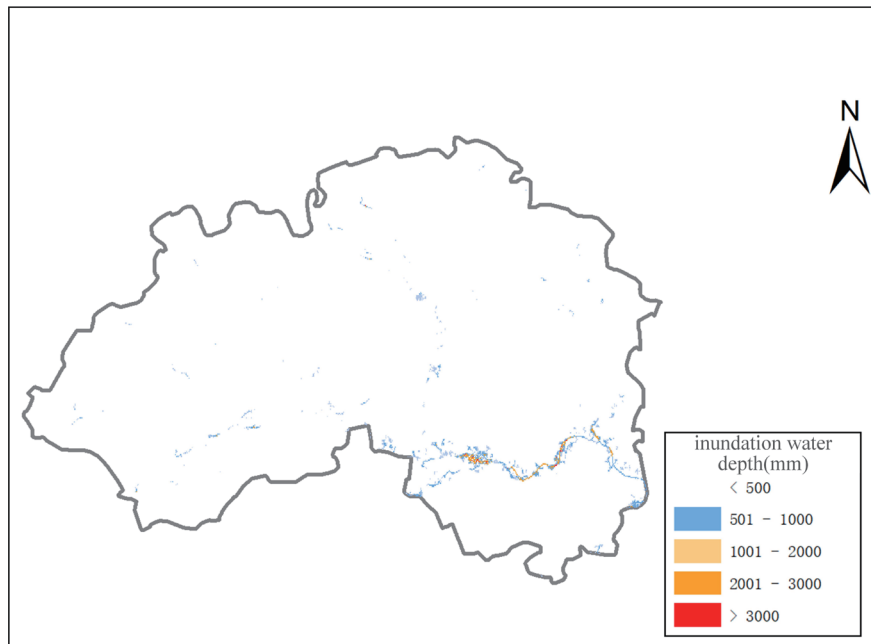


Fig. 8. (Color online) Distribution of inundation water depth from 8 pm July 23, 2023 to 8 pm August 6, 2023 in Changping District (mm).

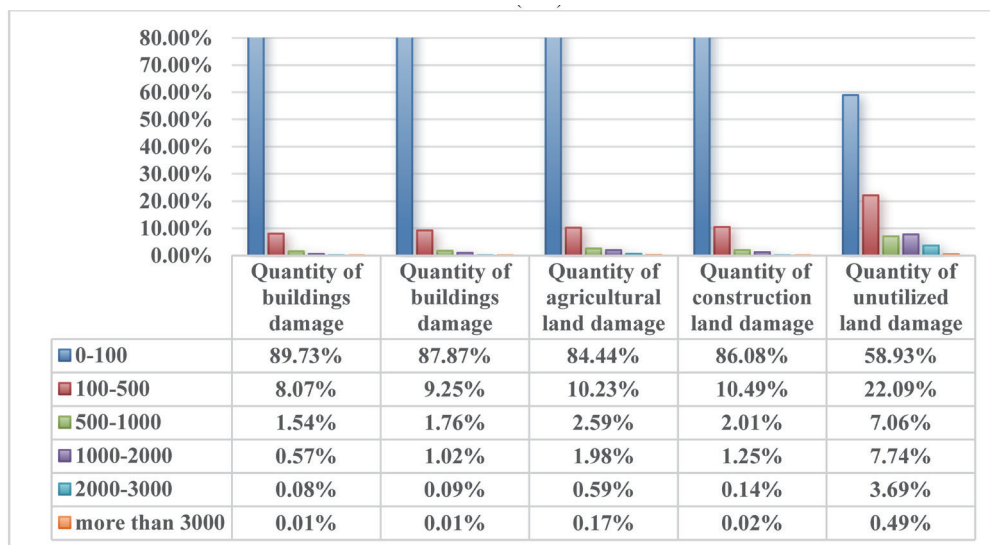


Fig. 9. (Color online) Changping District damage statistics.

### 3.2.3 Bridge risk analysis model results

On the basis of the bridge risk analysis model described in Sect. 2.1.4, we analyzed the correlation between damaged bridges and flood velocity. According to historical data, there are

249 bridges in Mentougou District and 843 bridges in Fangshan District. On the basis of remote sensing images, we analyzed the bridges damaged after heavy rainfall in Beijing. The manual analysis showed that 62 bridges were damaged in Mentougou District, 40 of which were completely damaged. In Fangshan District, 50 bridges were damaged, 33 of which were completely damaged. On the basis of the flow velocity data simulated by the damaged bridge and the model described in Sect. 2.1.2, we analyzed the correlation between the bridge and the flow velocity to evaluate the risk of the damaged bridge in the affected area.

### 3.2.3.1 Mentougou District hazard analysis of damaged bridges

During this round of heavy rainfall, the average flow velocity corresponding to all 249 bridges in Mentougou District was 0.17 m/s. However, the average flow velocity of the 62 damaged bridges in Mentougou District amounted to 0.79 m/s, which is about five times the average of all the bridges, indicating that the higher flow velocity had a certain impact on the damage of the bridges (Fig. 10).

The 22 partially damaged bridges corresponded to an average flow velocity of 0.29 m/s and a maximum of 1.57 m/s, but the 40 fully damaged bridges corresponded to an average flow velocity of 1.07 m/s and a maximum of 7.45 m/s, which is five times the flow velocity of the partially damaged bridges. Whether it is the mean or the maximum value, the flow velocity of the fully damaged bridges is significantly higher than that of the partially damaged bridges, which shows that the higher the flow velocity, the more serious the damage.

After statistical analysis, when the maximum flow velocity is greater than 0.01 m/s, the number of partially damaged bridges is 18, accounting for 80% of the total damage; when it is

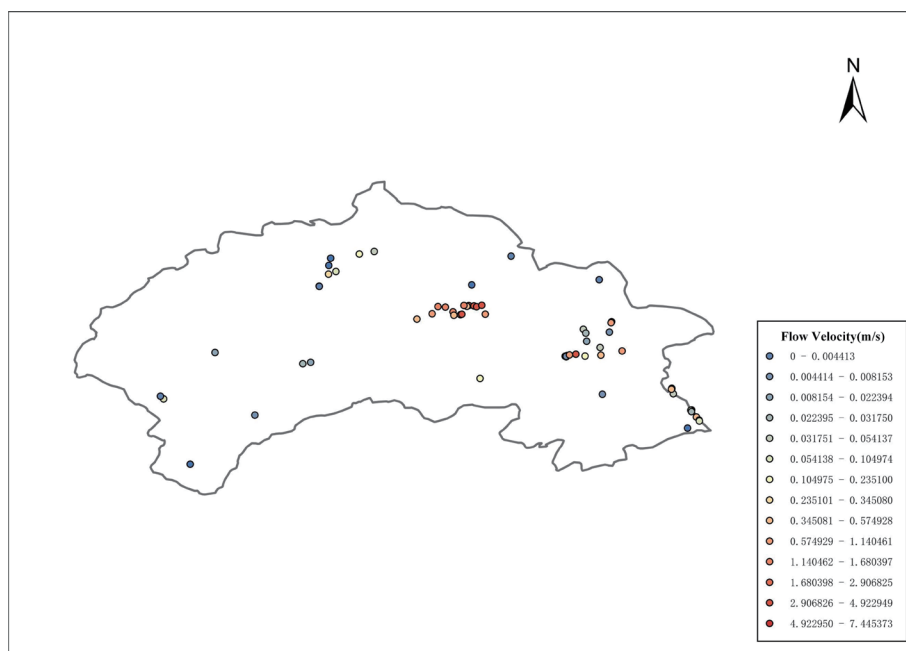


Fig. 10. (Color online) Distribution of flow velocities of damaged bridges in Mentougou District.

greater than 0.03 m/s, the number of partially damaged bridges accounts for 60% of the total damage and the number of completely damaged bridges accounts for 70% of the total damage. The specific relationship between the number of damaged bridges and the flow velocity is shown in Tables 1 and 2.

Considering the flow velocities of partially and completely damaged bridges, we selected 0.03 m/s as the critical flow velocity between damaged and undamaged bridges (the damaged quantity accounted for about 60% of the total damaged quantity), and by analyzing the flow velocity data of 249 bridges in Mentougou District, a total of 82 bridges that were subjected to considerable impacts were extracted, and excluding 62 damaged bridges in the remote sensing decipherment, there were 20 bridges that were also subjected to considerable impacts (Fig. 11).

Table 1  
Velocity distribution of bridges with minor damage in Mentougou District.

Velocity interval (m/s)	>0.07	>0.03	>0.02	>0.01
Percentage of minor damage to total damage (%)	50	60	70	80

Table 2  
Velocity distribution of bridges with severe damage in Mentougou District.

Velocity interval (m/s)	>0.19	>0.1	>0.03	>0.01
Percentage of severe damage to total damage (%)	50	60	70	80

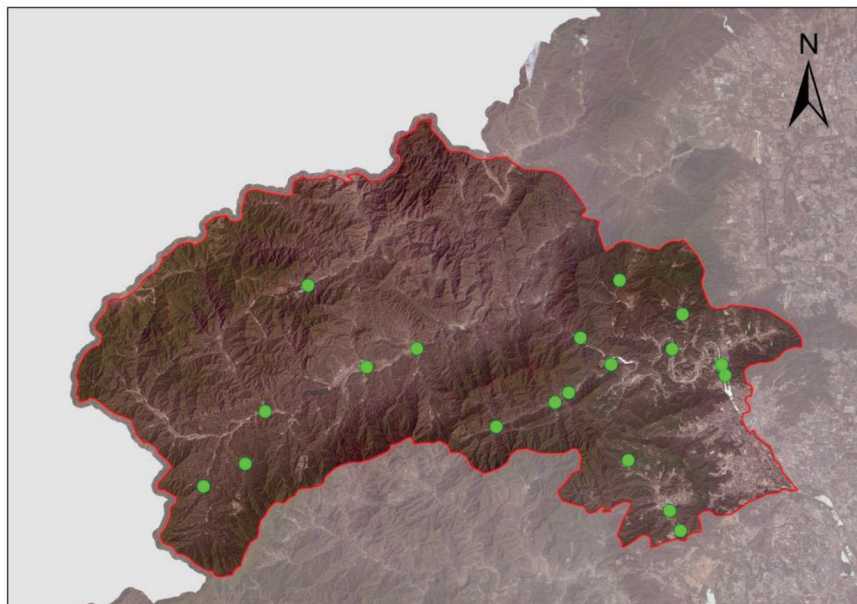


Fig. 11. (Color online) Spatial distribution of the remaining 20 bridges in Mentougou District that were subjected to considerable impacts (damaged bridges have been removed for deciphering).

### 3.2.3.2 Hazard analysis of damaged bridges in Fangshan District

During this round of heavy rainfall, the average flow velocity corresponding to all 843 bridges in Fangshan District was 0.05 m/s. However, among the 50 affected bridges in Fangshan District, the average flow velocity was 0.25 m/s, which is about five times that of all the bridges, suggesting that the higher flow velocity has a certain effect on the damage of bridges.

The average flow velocity of 17 partially damaged bridges is 0.24 m/s, and the maximum is 1.16 m/s. The average flow velocity of 33 completely damaged bridges is 0.27 m/s, and the maximum is 1.45 m/s. Both the mean and maximum flow velocities of the completely damaged bridges are much higher than those of the partially damaged bridges, which reflects the positive correlation between the flow velocity and the degree of damage of the bridges. This reflects that flow velocity is positively related to the damage degree of the bridge (Fig. 12).

After statistical analysis, when the flow velocity is greater than 0.01 m/s, there are 12 partially damaged bridges, accounting for 70% of the total damage, and 26 completely damaged bridges, accounting for 80% of the total damage. When it is greater than 0.03 m/s, the number of partially damaged bridges is 13, accounting for 60% of the total damage, and the number of completely damaged bridges is 23, accounting for 70% of the total damage. The relationship between the specific number of damaged bridges and the flow velocity is shown in Tables 3 and 4.

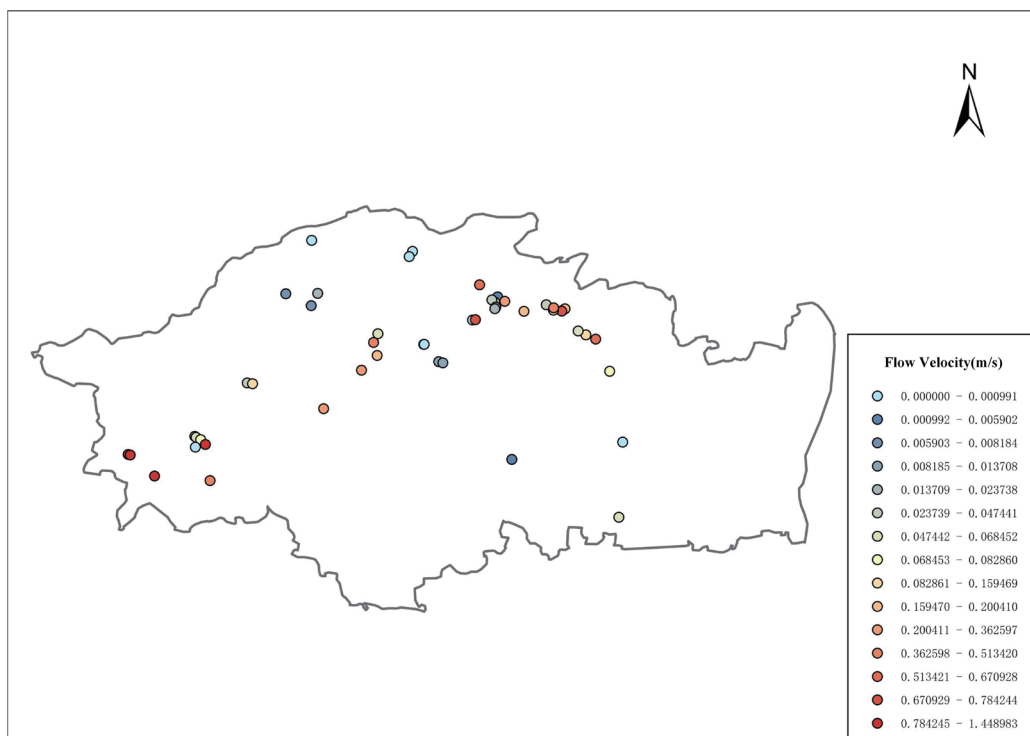


Fig. 12. (Color online) Distribution of flow velocities at damaged bridges in Fangshan District.

Table 3  
Velocity distribution of bridges with minor damage in Fangshan District.

Velocity interval (m/s)	>0.06	>0.03	>0.01	>0.005
Percentage of minor damage to total damage (%)	50	60	70	80

Table 4  
Velocity distribution of bridges with severe damage in Fangshan District.

Velocity interval (m/s)	>0.08	>0.07	>0.02	>0.01
Percentage of severe damage to total damage (%)	50	60	70	80

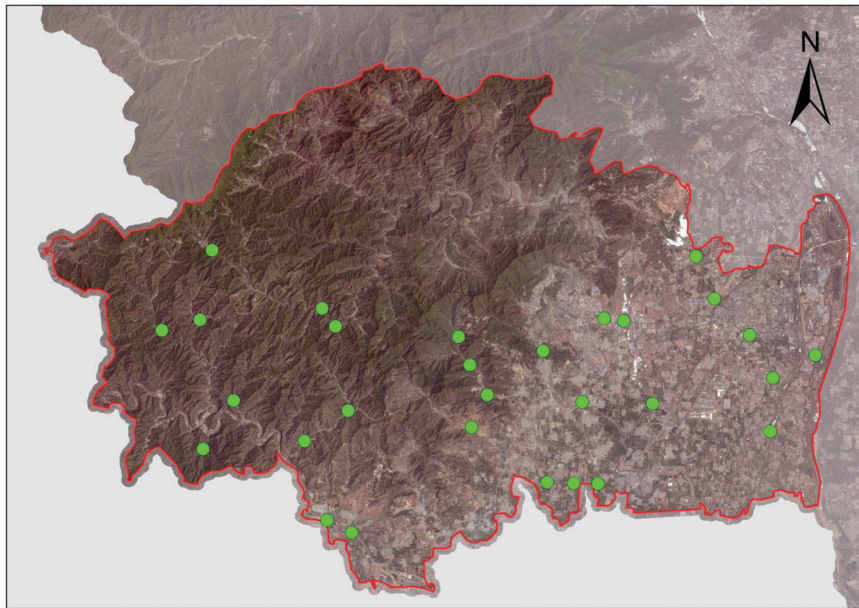


Fig. 13. (Color online) Spatial distribution of the remaining 32 massively impacted bridges in Fangshan District (damaged bridges have been removed for deciphering).

Considering the flow velocities of partially and completely damaged bridges, we selected 0.03 m/s as the critical flow velocity between the damaged and undamaged bridges (the number of damaged bridges accounts for about 60% of the total number of damaged bridges). By analyzing the flow velocity data of 843 bridges in Fangshan District, a total of 82 damaged Bridges were extracted. In addition to 50 damaged bridges with remote sensing images, 32 bridges were extracted through the correlation model in this paper (Fig. 13).

### 3.2.4 Results of disaster risk prediction analysis

The distribution of inundation water depths in Fangshan District at three-hour intervals from 0:00 a.m. on September 17 to 0:00 a.m. on September 18 (UTC time) simulated by the model in

Sect. 2.2 was used to form a nine-phase inundation water depth dynamics monitoring and warning map (as shown in Fig. 14). The comparative analysis of the inundation depth from 0:00 on September 17 to 0:00 on September 18 shows that the overall impact of this rainfall on Fangshan District is not significant. The possible areas with greater potential impact are located near Xiaoqing River, where the inundation depth in some areas exceeded 500 mm, except for other areas where the inundation depth did not exceed 500 mm. The inundation depth near Reject River was also only in the range of 200 mm, not exceeding 500 mm, but it may still have some impact on transportation and residents' lives, which can be prevented in the region.

On the basis of the predicted inundation water depths at 00:00 on September 18, we selected the inundation water depths of more than 200 and 500 mm as the thresholds for this damage assessment, and we used the dynamic damage assessment model described in Sect. 2.3 to conduct a damage analysis of the rainfall and assess the communities within the inundation area that might be affected by the rainfall. After counting, the number of communities and villages that may be affected by this rainfall with inundation depths exceeding 500 mm is 32, all of which are located near Xiaoqing River; the total number of communities and villages with inundation depths between 200 and 500 mm is 12. Through the field rainfall test, the accuracy

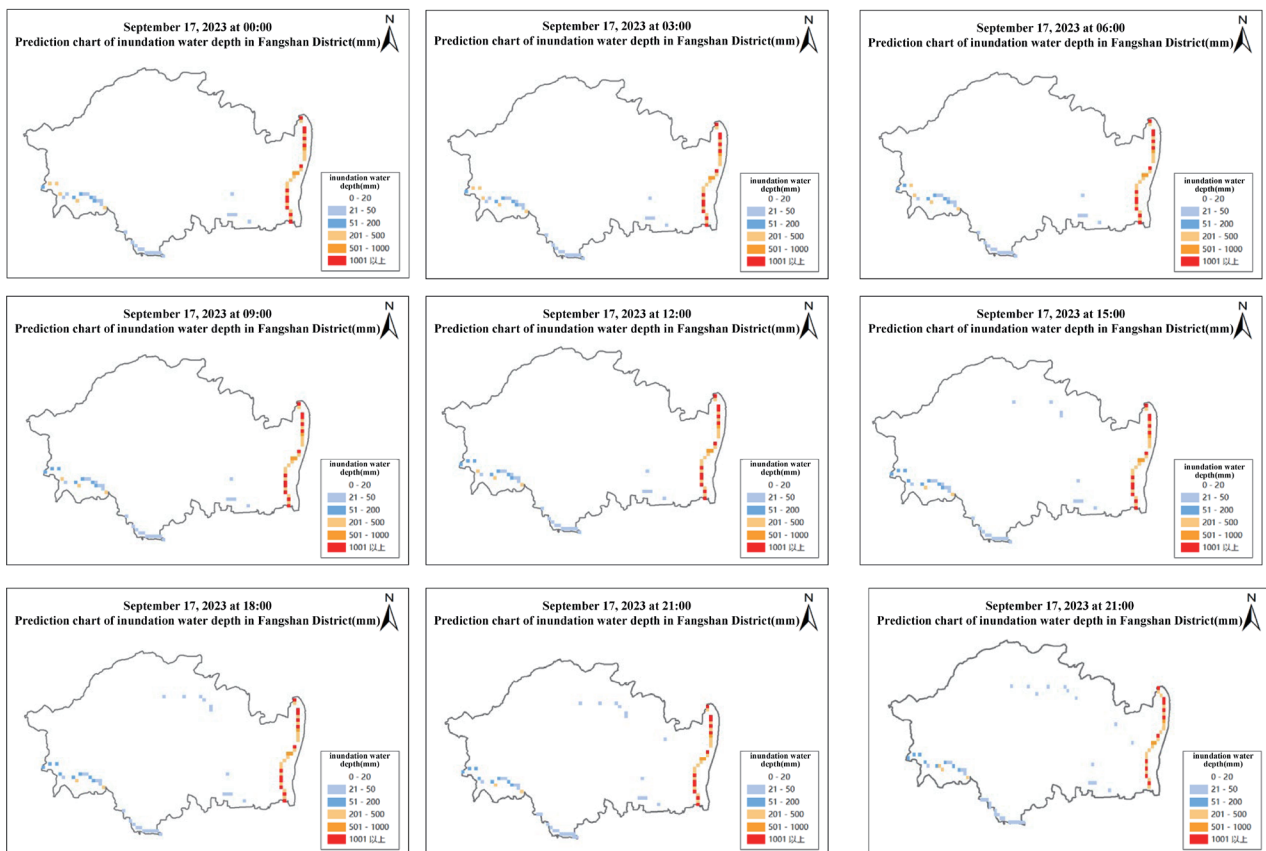


Fig. 14. (Color online) Dynamic monitoring of inundation water depth in Fangshan District on September 17, 2024.

rate of the model is higher than 70%, and the evaluation efficiency of the model has been further improved compared with manual interpretation.

#### 4. Conclusions

In view of the frequent occurrence of extreme meteorological disasters in recent years, in order to effectively assess and trace the losses caused by disasters, it is necessary to carry out disaster loss degree and risk analysis. Therefore, for rainstorm disaster risk assessment, we constructed the rainstorm disaster damage dynamic assessment and bridge risk assessment model and carried out the risk prediction and analysis of the disaster area before the rainfall. The main conclusions are as follows: (1) inundation area, inundation, depth, and flow velocity are simulated quickly by using the inundation simulation estimation model. After comparison with the radar image analysis results and manual judgment, the main trend of the simulated results was found to be basically consistent with the actual situation. (2) In terms of the degree of disaster loss, we constructed a dynamic assessment model of disaster loss, adopted spatiotemporal data and a hydrological model to carry out the disaster assessment of houses, land, and infrastructure, and effectively evaluated the quantity and spatial distribution of damaged houses, land, and infrastructure. (3) For disaster risk analysis, a bridge risk analysis model was proposed in this paper to analyze the correlation between bridge damage and flood flow velocity, and the analysis results basically showed that the maximum flow velocity has a strong positive correlation with the damage degree of bridges. Aside from the damaged bridges interpreted by remote sensing, other dangerous bridges after flood impact can be analyzed and calculated on the basis of this model. (4) On the basis of the results of the above analysis model, we predicted and analyzed the disaster situation in Fangshan District and analyzed the spatial distribution of areas potentially affected by rainfall to strengthen the disaster early warning work in this region. In addition, in the model calculation of disaster loss and bridge damage analysis in this paper, we found that the simulation accuracy depends on the terrain and other multisource data, and thus, the model accuracy in this paper has not been refined. In the future, the accuracy of model simulation and evaluation analysis will be improved by improving the terrain resolution, such as the accuracy of DEM.

#### References

- 1 J. M. Shepherd: *Earth Interact.* **9** (2005) 1. <https://doi.org/10.1175/EI156.1>
- 2 Z. Ding and L. Na: *China Flood & Drought Manage.* **28** (2018) 1. <https://doi.org/10.16867/j.issn.1673-9264.2018168>
- 3 Y. C. Tao: PEKING University (2019). <https://doi.org/10.19580/j.cnki.1007-3000.2019.07.029>
- 4 S. Weis, V. Agostini, and L. Roth: *Clim. Change.* **136** (2016) 615. <https://doi.org/10.1007/s10584-016-1642-0>
- 5 S. Hanson, R. Nicholls, and N. Ranger: *Clim. Change.* **104** (2011) 89. <https://doi.org/10.1007/s10584-010-9977-4>
- 6 A. Kebede and R. Nicholls: *Reg. Environ. Change.* **12** (2012) 81. <https://doi.org/10.1007/s10113-011-0239-4>
- 7 Y. Zhan, J. Yin, and S. Xu: *J. Geogr. Sci.* **21** (2011) 274. <https://doi.org/10.1007/s11442-011-0844-7>
- 8 G. Benito, M. Lang, and M. Barriandos: *Nat. Hazard.* **31** (2004) 623. <https://doi.org/10.1023/B:NHAZ.0000024895.48463.eb>
- 9 H. Mojaddadi, B. Pradhan, and H. Nampak: *Geomatics Nat. Hazards Risk.* **8** (2017) 1080. <https://doi.org/10.1080/19475705.2017.1294113>

- 10 L. Chun-Hong, L. Ren, Z. Zuo, and H. Jiang: Hydrol. (2005). [https://xueshu.baidu.com/usercenter/paper/show?paperid=18217348f92f9f99cfdb95dde8aa7f17&site=xueshu\\_se](https://xueshu.baidu.com/usercenter/paper/show?paperid=18217348f92f9f99cfdb95dde8aa7f17&site=xueshu_se)
- 11 L. Ting, S. Pei, and M. Chun: J. Beijing Normal University (Natural Science) **58** (2022) 300. <https://doi.org/10.12202/j.0476-0301.202124>
- 12 K. Gabriels, P. Willems, and V. Orshoven: Nat. Hazards Earth Syst. Sci. **22** (2022) 395. <https://doi.org/10.5194/NHESS-2021-51>
- 13 L. Yan, D. Han, and T. Hong: Adv. Meteorol. Sci. Technol. **10** (2020) 121. <https://doi.org/10.12202/j.0476-0301.202005018>
- 14 S. Yang, C. Chang, C. Hsu, and S. Wu: Nat. Hazard. **111** (2022) 2297. <https://doi.org/10.1007/s11069-021-05138-1>
- 15 H. Wu, J. Kimball, N. Mantue, and J. Stanford: Water Resour. Res. **47** (2011) W03517. <https://doi.org/10.1029/2009WR008871>
- 16 H. Wu, R. Adler, Y. Tian, G. Huffman, H. Li, and J. Wang: Water Resour. Res. **50** (2014) 2693. <https://doi.org/10.1002/2013WR014710>
- 17 H. Wu, J. Kimball, H. Li, M. Huang, L. Leung, and R. Adler: Water Resour. Res. **48** (2012) W09701. <https://doi.org/10.1029/2012WR012313>
- 18 Z. Wang and J. Li: Geomatics World **30** (2023) 595. <https://doi.org/10.20117/j.jsti.202304015>
- 19 T. Z. Wang, Y. H. Wang, S. Ma, M. Z. Zhao, L. Zhang, Z. Xue, Y. Ren, and R. Sun: Water Resour. Hydropower Eng. **53** (2022) 1. <https://doi.org/10.13928/j.cnki.wrahe.2022.07.001>

## About the Authors



**Kui Zhang** received his M.S. degree in 2021 from the School of Information Engineering, China University of Geosciences (Beijing). He is now an assistant engineer at the Beijing Institute of Surveying and Mapping, China. He focuses on comprehending SAR images. His specific research interests include data augmentation theory and SAR image information extraction by deep learning methods. ([504719347@qq.com](mailto:504719347@qq.com))



**Yingchun Tao** received her Ph.D. degree from Peking University in 2019. She is now a professorate senior engineer at the Beijing Institute of Surveying and Mapping, China. Her research interests are in new fundamental surveying and mapping, photogrammetry and remote sensing, and real 3D construction. ([527359590@qq.com](mailto:527359590@qq.com))



**Xuping Zhang** received her B.S. degree from Capital Normal University, China, in 2020 and her M.Eng. degree from Beijing University of Civil Engineering and Architecture in 2023. Since 2023, she has been an assistant engineer at the Beijing Institute of Surveying and Mapping, China. Her research interest is in remote sensing. ([915028935@qq.com](mailto:915028935@qq.com))



**Yanyan Zeng** received her B.S. degree from China University of Petroleum, Shandong, in 2010 and her Ph.D. degree from the University of Chinese Academy of Sciences, Beijing, in 2015. Since 2015, she has been a senior engineer at the Beijing Institute of Surveying and Mapping, China. Her research interests are in GNSS data processing and new fundamental surveying and mapping. ([zengyanyan1989@163.com](mailto:zengyanyan1989@163.com))



**Zongxia Xu** received her M.S. degree in geographic information engineering from Capital Normal University, China, in 2019. Since 2019, she has been working at the Beijing Institute of Surveying and Mapping, and since 2021, she has been an engineer. Her research interest is in remote sensing image interpretation. ([xuzongxia123@163.com](mailto:xuzongxia123@163.com))



**Hanmei Liang** received her M.S. degree in human geography from Capital Normal University, China, in 2012. She served as a college-graduate village official in Daxing District of Beijing from 2012 to 2015 and has been working at the Beijing Institute of Surveying and Mapping since July 2015. Her research interests are in mapping and geographic information.



**Yandi Zhou** received her M.S. degree in surveying and mapping engineering from Beijing University of Civil Engineering and Architecture, China, in 2022. Since 2022, she has been working at the Beijing Institute of Surveying and Mapping as an assistant engineer. Her research interest is in geographic information science. ([18610727227@163.com](mailto:18610727227@163.com)).